

Fabrication of Carbon Nanofibers/A356 Nanocomposites by High-Intensity Ultrasonic Processing



QING-JIE WU and HONG YAN

A356 alloy reinforced with carbon nanofibers (CNFs) was fabricated by high-intensity ultrasonic vibration processing. The microstructure and mechanical properties were investigated. The distribution of CNFs became more and more uniform with the increase of ultrasonic power, and the mechanical properties of nanocomposites were significantly enhanced accordingly. The yield strength (YS), ultimate tensile strength (UTS), and microhardness of the nanocomposite increased by 38.3, 21.9, and 43.2 pct, respectively, at a CNF content of 0.9 wt pct compared with the matrix without CNF addition. The improvement in mechanical properties was the effect of CNFs on the thermal expansion mismatch strengthening of the nanocomposite, the grain refinement of the nanocomposite, and the load transfer from the matrix to the nanofibers.

<https://doi.org/10.1007/s11661-018-4578-3>

© The Minerals, Metals & Materials Society and ASM International 2018

I. INTRODUCTION

HIGH-STRENGTH light structural materials have many applications, such as in construction, automotive, aviation, and many other industries. As a novel material, carbon nanofibers (CNFs) have attracted much attention due to their exceedingly high elastic modulus and tensile strength. In addition, most CNFs have a smooth surface, low curvature, and almost the same size of diameter, which promotes CNF dispersion uniformly in the matrix and provides great opportunities for industrial applications.^[1,2] Therefore, the CNFs are a candidate with great potential as reinforcement of composites for mass production. At present, various efforts have been made to develop CNFs as a reinforcement for metal matrix. Patchara *et al.*^[3] produced a Ti64/CNFs composite by a powder metallurgy process. They reported that the addition of nanofibers improved the tensile strength of composites. However, the elongation decreased due to the formation of brittle phases and microcracks. Fumio *et al.*^[4] fabricated CNF-reinforced aluminum matrix composites using sintering and hot extrusion. They reported that the mechanical properties of fabricated composites were also

significantly improved due to the CNFs, and the properties can be accurately predicted by proposed theoretical models.

At present, metal casting and power metallurgy are commonly used for the preparation of metal-based composite materials.^[5,6] However, powder metallurgy is not suitable for large-scale industrial production because of its high cost and processing difficulties. In contrast, the casting process has the advantages of low cost and easy operation, making it easier to adapt to modern industrial production requirements. However, a limited number of studies have been conducted on the fabrication of CNF-reinforced aluminum matrix composites produced by melt casting.

Conventional agitation casting is a relatively simple alternative process that can be used to produce metal matrix composites with complex shapes. Micron-sized particles can be successfully entrained into the melt by agitating vortex.^[7] However, nanosized reinforcements are difficult to disperse into the melt by the conventionally used stirring, due to their large surface area-to-volume ratio.^[8,9]

When treated by high-intensity ultrasound, the melt can generate acoustic cavitation and acoustic convection. The sound pressure gradient causes microstirring of the solution at high temperatures. The alternating pressure produced by ultrasound creates numerous cavities in the liquid metal. Parts of these cavities collapse under the compression stresses of the sound wave. When these cavities collapse, small areas of high pressure differences are generated, resulting in transient high pressure and cumulative jets.^[10–12] In addition, the rise of local temperature and the acceleration of

QING-JIE WU and HONG YAN are with the School of Mechanical and Electrical Engineering, Nanchang University, Nanchang, 330031, China and also with the Key Laboratory of Light Alloy Preparation & Processing in Nanchang City, Nanchang, 330031, China. Contact e-mail: hyan@ncu.edu.cn

Manuscript submitted April 24, 2017.

Article published online March 20, 2018

molecular movement resulting from ultrasound decrease viscosity and surface tension in the system, enhancing the wettability between the metal melt and the fibers, thus permitting uniform dispersion in the matrix.^[13–15]

In this article, we chose CNFs as reinforcements to fabricate aluminum composites. The base material was A356 aluminum alloy. CNFs/A356 aluminum matrix composites were prepared by casting and subjecting the matrix to high-intensity ultrasound. The effects of the ultrasonic power and CNF content on the preparation of the CNFs/A356 composites were investigated.

II. EXPERIMENTAL PROCEDURES

Commercial Al-7Si-Mg (A356) aluminum alloy was chosen as the matrix material, whose chemical composition is shown in Table I. In this study, we used CNFs with the following properties: purity over 98 pct, a diameter of 50 to 200 nm, and length of 3 to 12 μm (scanning electron microscope (SEM) image presented in Figure 1). To remove the residual catalyst and amorphous carbon from the surface, these fibers were heated at 3000 °C for 5 hours using a graphite resistance furnace operating in a vacuum atmosphere.

As shown in Figure 2, the experimental nanomanufacturing setup consists of an electric resistance furnace, an ultrasonic vibration device, and control parts. In this process, A356 was melted in a small corundum crucible of 50-mm diameter and 75-mm height using the furnace. The titanium waveguide, which was coupled with a 20 kHz, 600 to 3000 W ultrasonic converter (NP-C-20-3000VA), was dipped into the melt for ultrasonic processing. The aluminum melt pool was protected by argon gas.

First, CNFs were added into pure ethanol (99.7 pct purity) and dispersed with an ultrasonic disperser (PS-40) for about 20 to 30 minutes. Next, the corresponding aluminum powders were homogeneously added, and the sonication was continued for another 30 minutes. The ethanol solution containing aluminum powder and CNFs was then dried in a vacuum-drying oven at 60 °C for 48 hours. Finally, the resulting mixture was compacted under a pressure of 150 MPa and extruded at 653 K (380 °C) at an extrusion ratio of 40:1 to fabricate a 6 pct CNFs/A356 rod-shaped nanomaster alloy with a diameter of 6 mm. The obtained nanomaster alloy was divided into small rods with length of 5 to 10 mm (as shown in Figure 2).

The A356 alloy was melted at 750 °C in a corundum crucible by using a resistance furnace. Then, the Al-CNFs nanomaster alloy rods were inserted one by one into the A356 alloy melt. After the nanomaster alloy was completely melted, the melt was subjected to high-intensity ultrasonic treatment for 10 minutes in

Ar atmosphere (as shown in Figure 3). The A356 matrix fabricated under the optimal ultrasonic process parameters was evaluated for comparison. The content of fibers in the CNFs/A356 nanocomposites fabricated was controlled by the added amount of the nanomaster

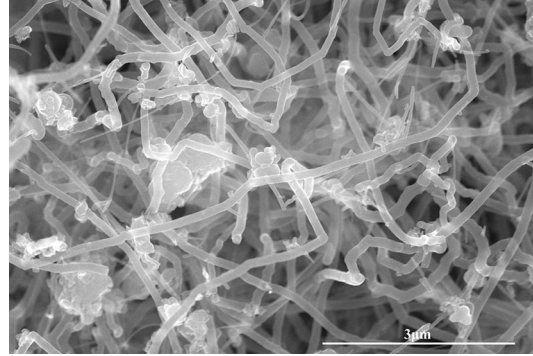


Fig. 1—SEM image of CNFs.



Fig. 2—Image of the Al/CNFs master alloy.

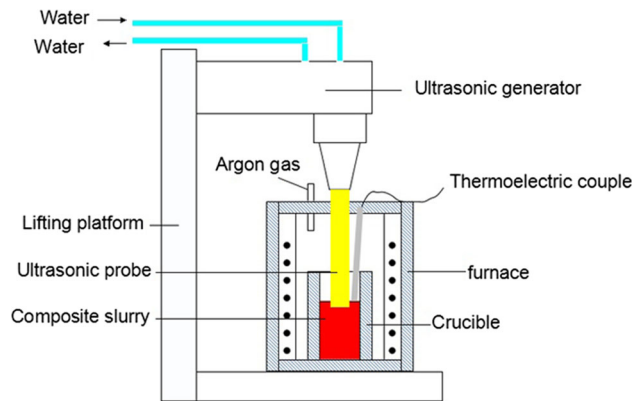


Fig. 3—Experimental setup for fabrication of CNF-reinforced aluminum matrix composites.

Table I. Chemical Composition of A356 Alloy (Weight Percent)

Element	Al	Si	Mg	Fe	Zn	Mn	Cu
Wt pct	balance	7.1	0.46	0.11	0.06	0.05	0.03

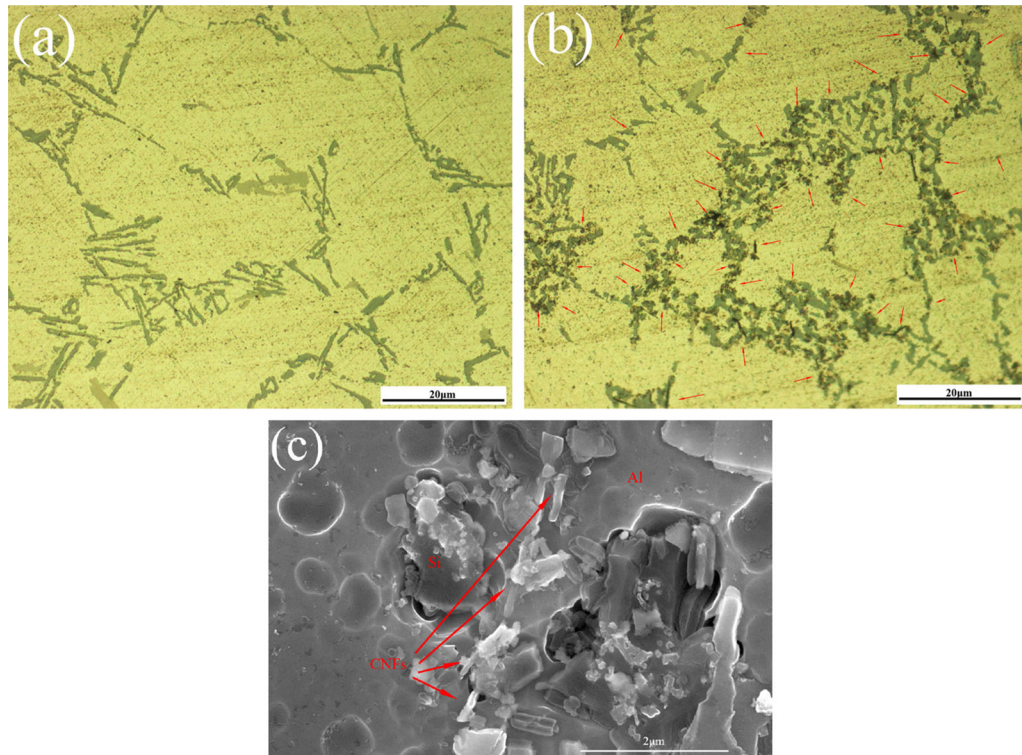


Fig. 4—Microstructures of the (a) pure A356 alloys and (b) CNFs/A356 nanocomposites with the addition of 0.9 wt pct CNFs. (c) SEM of nanocomposites with addition of 0.9 wt pct CNFs.

alloy. After the ultrasonic treatment, the composite was deslagged and poured into a preheated mold (400 °C).

Optical microstructures of the CNFs/A356 nanocomposite samples were examined using an optical microscope (Nikon ECLIPSE MA200) and an SEM (NOVA NANOSEM 450) after being etched by 0.5 vol pct hydrofluoric acid in water. The CNF/A356 interface was studied with a transmission electron microscope (TEM, JEM-2100). The hardness of the sample was measured by a microscopic Vickers hardness tester (HVS 1000A), applying a load of 0.3 kg with a load time of 15 seconds. The hardness result of each sample was the even value of 10 times. Tensile tests were carried out using a universal testing machine to investigate the strengthening effect of different CNF contents. Test samples with a diameter of 10 mm and a gage length of 50 mm were prepared in accordance with China Standard GB/T228-2002. The experimental speed was set at 0.5 mm/min. The fracture surfaces were then examined by an SEM.

III. EXPERIMENTAL RESULTS

A. Microstructural Characterization

The microstructures of the alloys with and without CNFs fabricated by the method of nanomaster addition under ultrasonic vibration were examined by optical microscopy, as shown in Figures 4(a) and (b), respectively. It can be noted in Figure 4(a) that typical coarse, platelike eutectic silicon was distributed along the grain

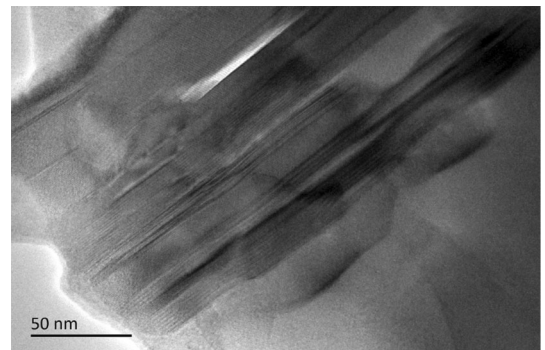


Fig. 5—TEM image of CNFs in the composite.

boundaries of the α -Al matrix. Also, it can be clearly seen in Figure 3(b) that large amounts of gray-black phase adhered to the eutectic silicon in the nanocomposites. The SEM image of the composite in Figure 4(c) shows that many rod-shaped nanoparticles were distributed near the grain boundaries or kept a buried state in grains. The sizes of nanoparticles were roughly equal to the CNFs, and the particles were well bound with the matrix.

Figure 5 displays the TEM images of typical CNFs in the fabricated composite. The multiwall structure of CNFs is clearly visible in this high-resolution TEM image, and its well-straight shape was retained in the composite. Figure 5 shows that the interfaces of the CNFs and Al are sound. Additionally, in the present TEM morphology, no sufficient evidence supported the

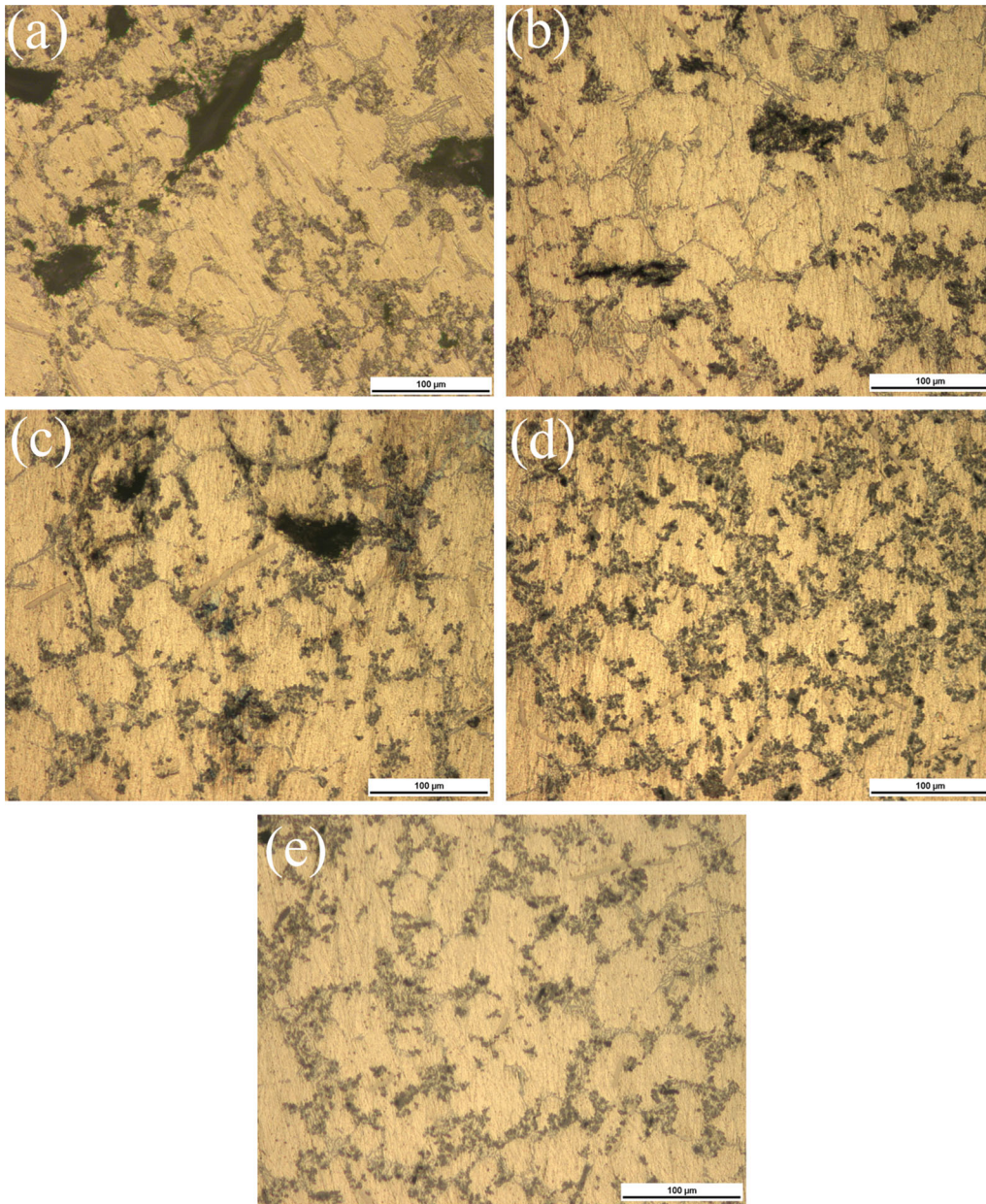


Fig. 6—Optical micrographs of the 0.9 wt pct CNFs/A356 nanocomposites fabricated using different ultrasonic power (kW): (a) 0, (b) 0.7, (c) 1.4, (d) 2.1, and (e) 2.8.

view of formation of Al_4C_3 phases on the interface. Huang *et al.*^[16] also reported that Al_4C_3 phases were not found between the interface of CNTs and Al, possibly because the high-intensity ultrasonic treatment suppressed the formation of Al_4C_3 phases.

Figure 6 presents the optical microstructures of CNFs/A356 composites (0.9 wt pct) fabricated under various ultrasonic power. For comparison, the composite was also prepared using mechanical agitation at a speed of 400 rpm for 6 minutes under Ar atmosphere. Its optical microscopy image is shown in Figure 6(a), where black zones are unevenly distributed in the nanocomposites. In contrast, the dark CNF aggregation was homogeneously distributed along the grain boundaries after treatment by high-intensity ultrasound in

Figures 6(b) through (d). The quantity of black zones increases with increasing ultrasonic power, while the size of the zones decreases. As shown in Figure 6(d), the use of ultrasonic power of 2.1 kW contributes to the best dispersion. It means that as the ultrasonic power increases, the dispersion of CNFs is improved. However, the microstructure of nanocomposite was almost unchanged or even the size of grain exhibited a slight increase trend when the ultrasonic power reached 2.8 kW, as shown in Figure 6(e).

Sautera *et al.* reported that^[9,12] under ultrasound treatment, the melt was generally subjected to a random compression-expansion cycle. The trapped gas in the CNF clutters serves as a nucleus for ultrasonic cavitation. Then, the cavitation bubbles progressively grow

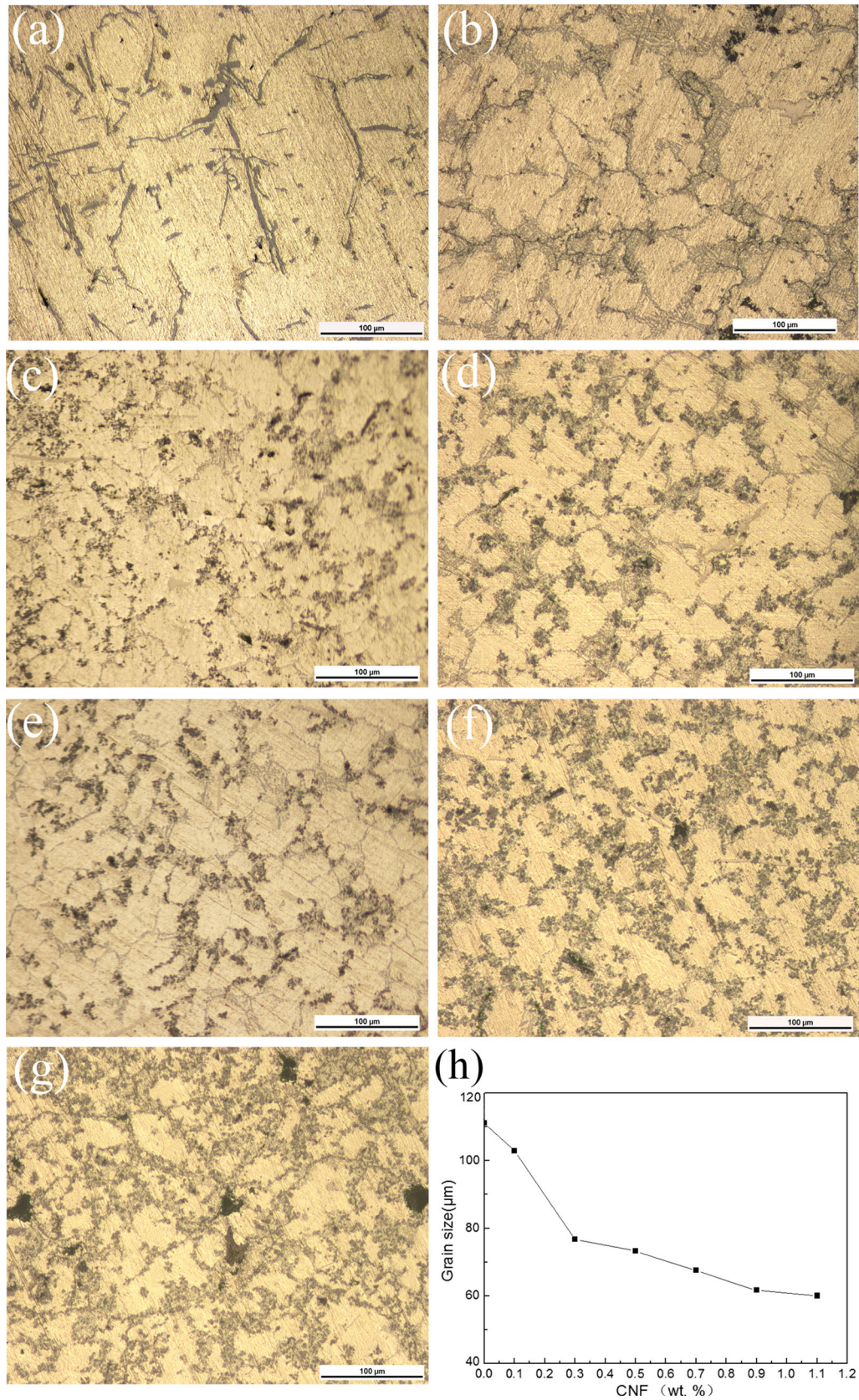


Fig. 7—Optical micrographs of the CNFs/A356 nanocomposites containing (a) 0.1 wt pct, (b) 0.3 wt pct, (c) 0.5 wt pct, (d) 0.7 wt pct, (e) 0.9 wt pct, and (f) 1.1 wt pct of CNF (g) fabricated at 2.1 Kw. (h) Grain size of CNFs/A356 nanocomposite.

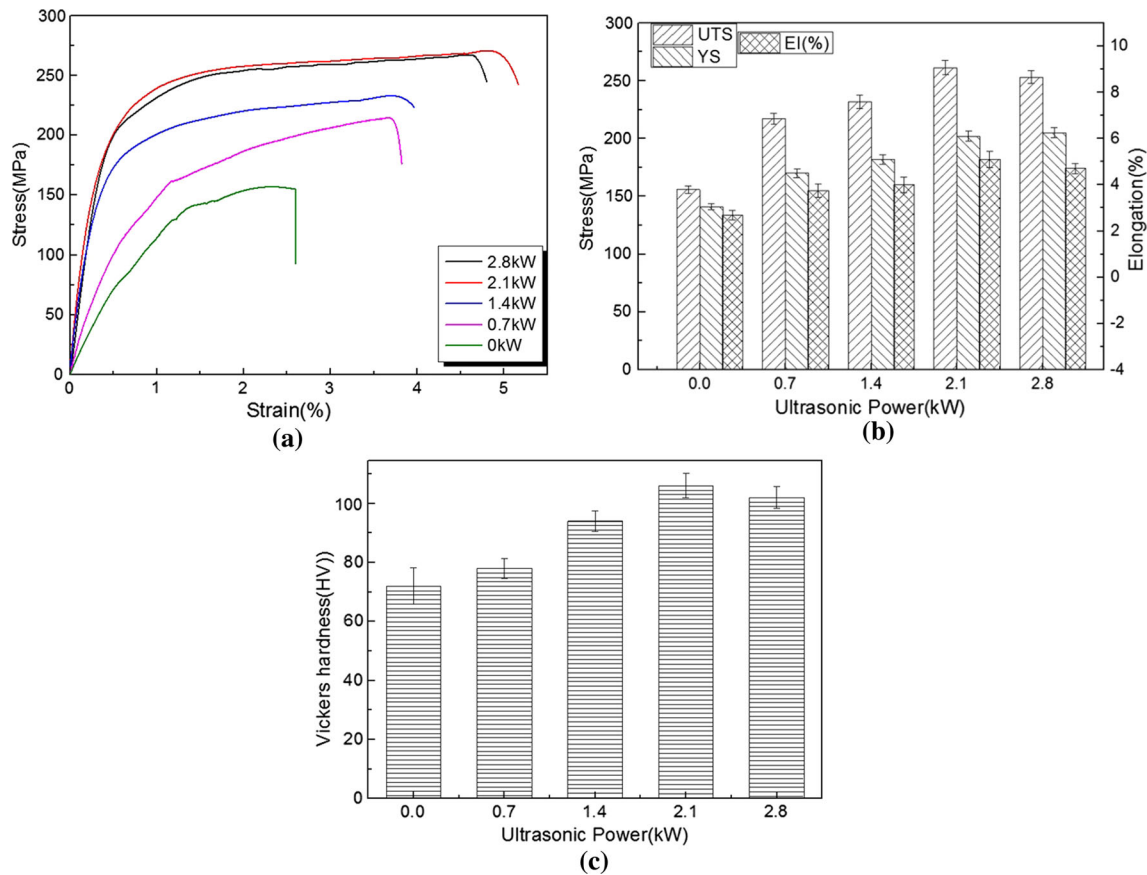


Fig. 8—(a) Tensile stress-strain curves, (b) tensile properties, and (c) Vickers hardness of CNFs/A356 nanocomposites prepared using treatments with different ultrasonic power.

and collapse under the influence of the compression-expansion cycle. This process produces localized high pressure and ultrahigh temperature, which leads to the dispersion of CNF aggregates. On the other hand, the high pressure and temperature also bring much energy to the melt, which improves the wettability between the CNFs and the matrix.^[13–15] Moreover, ultrasound provides the possibility of refining the matrix alloy microstructure due to the cavitation and acoustic streaming effect of ultrasound. The total effect of various kinds of streams is to vigorously mix and so homogenize the melt.^[17]

In the present study, the nanomaster alloy melted at the high temperature and released CNFs, which were then rapidly dispersed by the strong cavitation and the cavitation bubbles generated by the high-intensity ultrasound (Figure 6). This indicates that the continuous microcavitation in the melt caused by continuous ultrasonic treatment can disperse CNFs effectively. Furthermore, with increasing ultrasonic power, α -Al dendrites became more and more refined, as shown in Figure 6(c).

The microstructural characterization of CNFs/A356 nanocomposites prepared under ultrasonic power of 2.1 kW with various additions of CNF is presented in Figure 7. Dendritic-like silicon and dark phases can be clearly observed. It can also be noted that the quantity of the dark phase in the composite gradually increases

with the increasing content of CNFs. No obvious agglomeration can be detected in composites with CNF content less than 0.9 wt pct. This means that the CNFs with a low content can be dispersed effectively by ultrasonic processing. However, when the content reaches 1.1 wt pct, the microstructure of the nanocomposite shows a few agglomerations, as can be seen from Figure 7(g).

Average grain sizes of composites with various contents of CNFs calculated by IPP software are shown in Figure 7(h). With increasing content of CNFs from 0.1 to 0.9 wt pct, average grain size of the composites was gradually decreased. This indicates that CNFs have a significant effect on the grain refinement of A356 matrix. However, a further increase of the content of CNFs up to 1.1 wt pct has little effect on grain size, and clusters of CNFs were clearly observed on the grain boundary in Figure 7(g).

B. Mechanical Behavior

Figure 8 shows the mechanical behavior of 0.9 wt pct CNFs/A356 nanocomposites fabricated with various ultrasonic power. It can be concluded from Figures 8(a) and (b) that the tensile properties and elongation ratio of the nanocomposites were significantly improved with the increase of the ultrasonic power. The tensile strength, yield strength (YS), and elongation ratio of

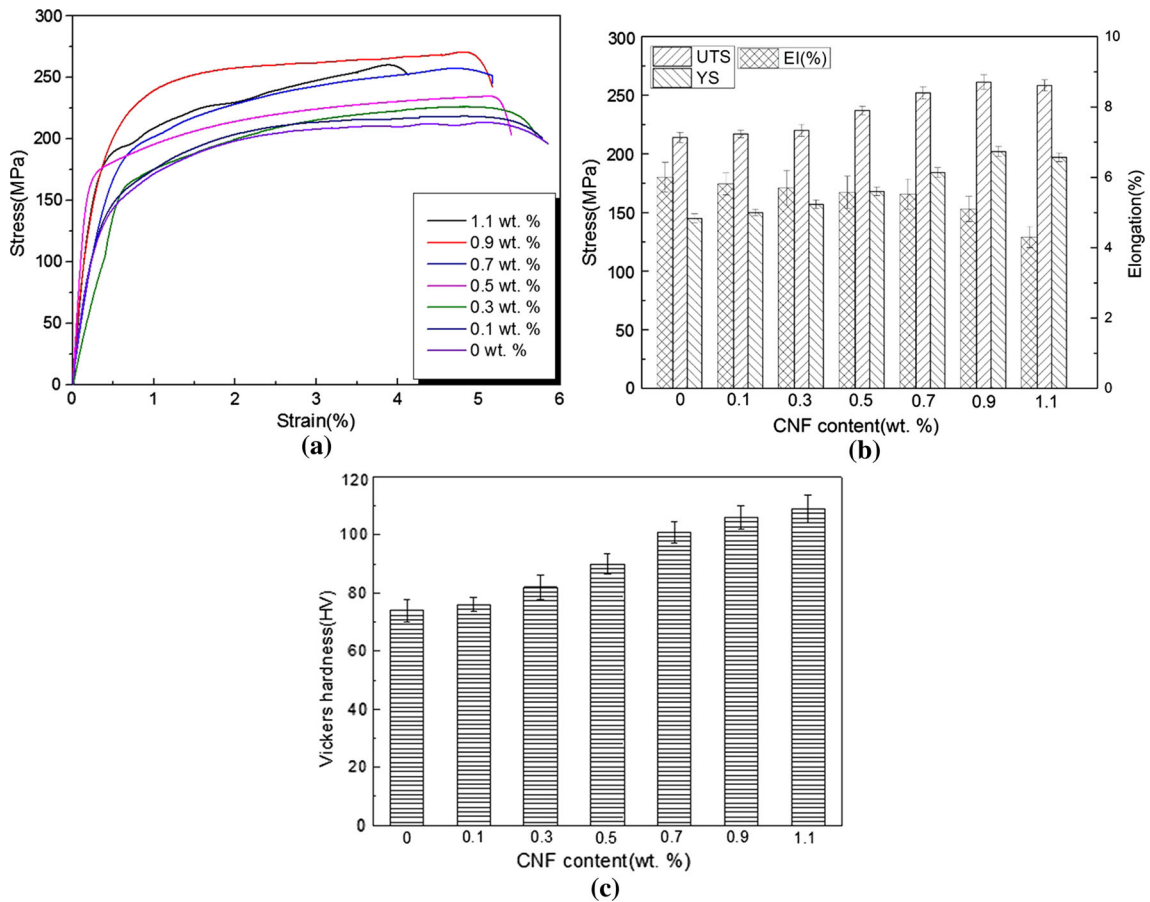


Fig. 9—(a) Tensile stress-strain curves, (b) tensile properties, and (c) Vickers hardness of CNFs/A356 nanocomposites prepared with different CNF content at 2.1 kW.

the composite were improved, and at 2.1 kW, the values of these indices reached 261, 202 MPa, and 5.1 pct, respectively. Compared with the CNFs/A356 nanocomposites prepared without ultrasonic treatment, the tensile strength, YS, and elongation of the composite were increased by 67, 43, and 89 pct, respectively. The diagram in Figure 8(b) indicated that the microhardness of the composites was also significantly improved with the increase of the ultrasonic power. However, when the ultrasonic power reached 2.8 kW, the tensile strength, YS, and elongation of the nanocomposite decreased to 253, 200 MPa, and 4.7 pct, correspondingly. It is noteworthy that ultrasonic power exerted effects on the microhardness of the 0.9 wt pct CNFs/A356 nanocomposites, which can be seen in Figure 7(c). The microhardness of the composites prepared was significantly improved with the increase of the ultrasonic power also. The microhardness of the 0.9 wt pct CNFs/A356 nanocomposites fabricated with the application of ultrasonic vibration at 2.1 kW is 106 HV, which was an increase of 47 pct compared to the composite without ultrasonic treatment. In addition, mechanical properties of the nanocomposites fabricated with ultrasonic vibration at 2.8 kW slightly decreased compared to 2.1 kW. The tensile strength, YS, and elongation of the nanocomposite were 253, 200 MPa, and 4.7 pct, respectively. Possibly, the thermal effect caused by ultrasonic

treatment could result in the decrease of cooling rate of the melt, thereby accelerating the grain growth and weakening the effect of grain refinement.^[18]

Excellent mechanical properties are related to the sound microstructure. It can be seen from Figures 6(a) through (c) that some large-size agglomerated CNFs appeared when the ultrasonic was less than 0.9 kW. The fiber aggregation or the worse bonding between CNFs and matrix produces brittle fracture easily because microcracks are initially formed around the conglomerations, which eventually result in deterioration of the mechanical properties. Meanwhile, the increase of ultrasonic power hindered CNF aggregation and the CNFs were more and more uniformly distributed, as shown in Figure 6. The reinforcements act as an obstacle of the slipping of dislocation, leading to an improvement of tensile strength.^[19]

The mechanical properties of the nanocomposites with different CNF content fabricated using ultrasonic vibration at 2.1 kW are shown in Figure 9. The microhardness of the matrix without CNFs fabricated by ultrasonic processing at the same power was 74 HV, and the ultimate tensile strength (UTS), YS, and elongation values were 214, 146 MPa, and 6 pct, respectively. The UTS and YS of the nanocomposite with CNFs of 0.9 wt pct content were 261 and 202 MPa, correspondingly. The microhardness, UTS, and YS values of the

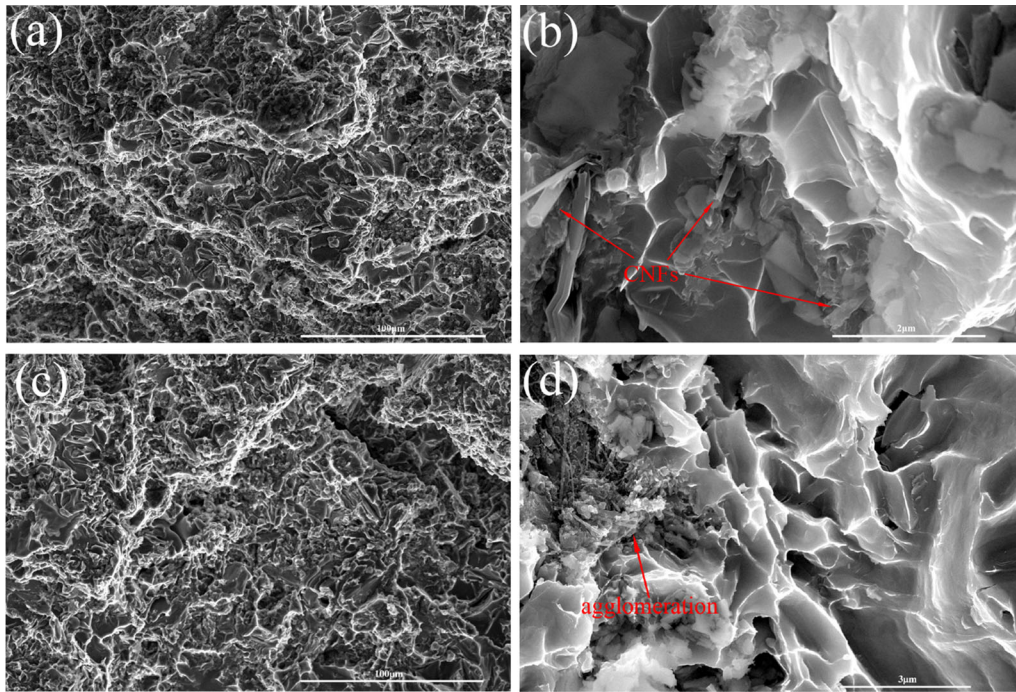


Fig. 10—SEM images of fracture surfaces: (a) and (b) 0.9 wt pct CNFs/A356; (c) and (d) 1.1 wt pct CNFs/A356.

nanocomposite were increased to 43.2, 21.9, and 38.3 pct, respectively, higher than those of the unreinforced A356 alloy. This can be attributed to the fact that CNFs could be effectively dispersed by a high-intensity ultrasonic process. The elongation of the nanocomposite exhibits a slight decrease trend, possibly due to agglomeration^[20] and pinning effect. The reinforcement or grain boundaries act as an obstacle to dislocation movement. The occurrence of grain refinement leads to the increase of the grain boundaries so that the dislocation slip of adjacent grains is more difficult to be driven. Nevertheless, the mechanical properties declined slightly when the content of CNFs reached 1.1 wt pct. This can be attributed to the agglomeration occurring in composite that promotes the formation of microvoids.^[16]

C. Fracture Characteristics

SEM images after the tensile tests of the fracture surface of nanocomposites with 0.9 wt pct CNFs prepared at 2.1 kW are shown in Figures 10(a) and (b). In Figure 10(a), except few quasi-cleavage planes, the fractured surface of the composite was characterized by many dimples. This indicated that the main fracture mechanism was ductile fracture. As shown in Figure 10(b), some nonagglomerated CNFs were depicted on the fracture face. This phenomenon indicates that CNFs were homogeneously distributed in the matrix, which corroborates the effectiveness of ultrasound treatment.

SEM images of the fracture surface of aluminum matrix composites with 1.1 wt pct CNFs prepared by ultrasonic vibration at 2.1 kW are shown in Figures 10(c) and (d). The fracture surface of

nanocomposites in Figure 10(c) also displays several dimples. However, the quantity of the quasi-cleavage planes significantly increases, and even a microcrack appears on the fracture face. As a result, the ductility decreased slightly when the CNF content exceeded 0.9 wt pct. As can be seen from Figure 10(d), some agglomerated CNFs appears on the fracture surface, which has a negative impact on the mechanical properties of the nanocomposites.

IV. DISCUSSION

The coefficient of thermal expansion^[21] of CNFs is $-1.5 \times 10^{-6} \text{ K}^{-1}$. Pure aluminum, however, has an extremely large coefficient of thermal expansion of $23.6 \times 10^6 \text{ K}^{-1}$. Hence, there is a considerable mismatch in the coefficient of thermal expansion between the CNFs and the aluminum matrix, resulting in prismatic punching of dislocation at the interface. The resulting dislocation density is dependent on the reinforcement surface area. The smaller the diameter of the fibers, the higher is the dislocation density. This phenomenon would result in the enhancement of the material properties in turn.

Dislocation density^[22] ρ is given by

$$\rho = 10A\varepsilon/(bt(1-A)) \quad [1]$$

where t is the diameter of the reinforcement (CNFs), b is the Burgers vector, ε is the thermal strain, and A is the volume fraction of reinforcement (CNFs).

The theoretical YS^[22] of the composites is

$$\Delta\sigma = \alpha\mu\rho^{(1/2)}b \quad [2]$$

where $\alpha = 1.25$, μ is the shear modulus of the matrix (Al), and \mathbf{b} is the Burgers vector.

It can be noted from Eq. [2] that the increment of intensity is proportional to the square root of dislocation density. Equation [1] shows that the dislocation density depends on the value of the volume fraction and the diameter of the reinforcement when the thermal strain of reinforcement is a constant. One of the advantages of CNFs is their small diameter compared with conventional fibrous materials, which, according to Eq. [1], causes the emergence of many dislocations (shown in Figure 11) and, thus, leads to the improvement of the mechanical properties of the nanocomposites.

On the other hand, the addition of CNFs results in the decrease of grain size, which causes the increase of YS of the nanocomposites. The reason is that the CNFs with a volume fraction form the network along the grain boundaries. Therefore, the grain growth of matrix is efficiently restrained by the Zener pinning effect.^[23,24]

The enhancement of mechanical properties of the composites is due to the decrease of grain size, which can be calculated by the following Hall–Petch^[23] equation:

$$\Delta\sigma_{\text{Hall-Petch}} = k(d_{\text{com}}^{-1/2} - d_{\text{alloy}}^{-1/2}) \quad [3]$$

where d_{com} and d_{alloy} are the average grain sizes of the composite and the alloy, respectively, and k is the Hall–Petch coefficient of A356 alloy. The YS of the composites increases with increased content of CNFs.

As shown in Figure 9, when the content of CNFs is less than 0.9 wt pct, the trend of YS is in accordance with Eq. [3]. However, the YS of the nanocomposites decreased when the content of CNFs exceeded 0.9 wt pct. Perhaps the presence of the agglomeration leads to the generation of microcracks.^[16] The homogeneous distribution of CNFs is a key factor for enhancing the mechanical properties of nanocomposites.^[24]

In addition, because the CNFs bonded well with the matrix, the applied force was transmitted from the matrix to the fibers by the shear stresses formed along the interface. The Kelly–Tyson model^[25] is often used to calculate the UTS of CNFs/A356 nanocomposites to further analyze the strength of the mechanical properties of the composites when neglecting the grain size effect. This model is valid for aligned fibers in the loading direction.

$$\sigma_c = \sigma_f V_f \left(1 - \frac{l}{2l_c}\right) + \sigma_m (1 - V_f) \quad [4]$$

where V_f is the volume fraction, σ_f is the strength of the fiber, and σ_m is the strength of the matrix. In this study, σ_f is assumed to be 13 GPa.^[3] According to the volume-mass conversion, a volume content of 0.18 to 1.9 pct can be obtained from the mass fraction of CNF contents in composites. σ_m is equal to 214 MPa, l is the average fiber length, and l_c is the length of the fiber when the composite is broken.

In conventional calculation, l_c is usually replaced by the average fiber length and the theoretical value is

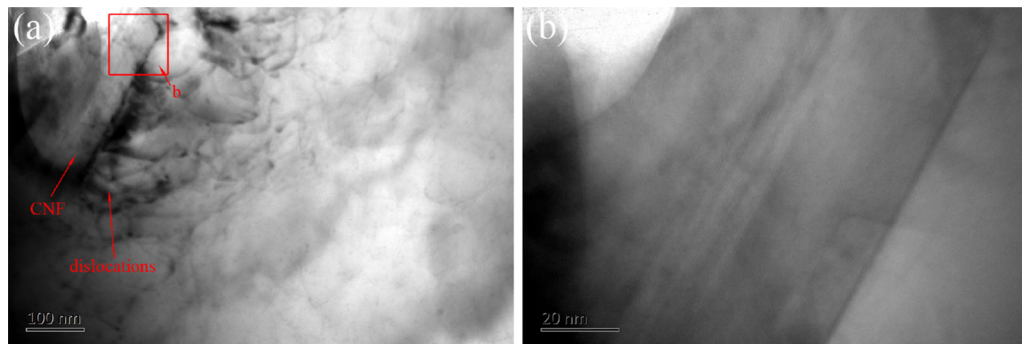


Fig. 11—TEM images of dislocations found in the 0.9 wt pct CNFs/A356 nanocomposites and the interface of CNFs and Al: (a) the dislocation and the CNF and (b) a high-magnification TEM image for the CNF.

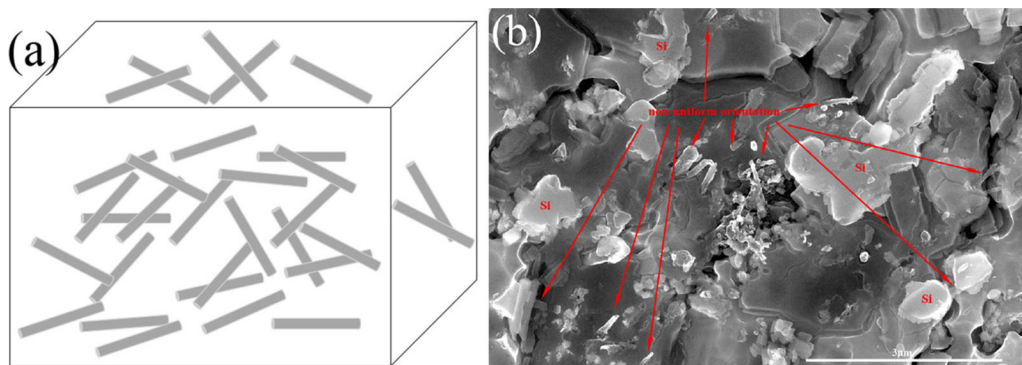


Fig. 12—(a) Schematic presentation of CNFs in nanocomposite and (b) SEM of the nanocomposite with 0.9 wt pct CNFs prepared at 2.1 kW.

calculated to be 225 to 334 MPa. These values are higher than the ones obtained in the tensile test. Based on the uniform distribution of the fibers, the dislocation mechanism and the fiber-reinforced mechanism can be used to determine the mechanical properties. Particularly, the Kelly–Tyson model is based on the perfect alignment of the fibers in the loading direction without the appearance of agglomeration. However, as shown in Figure 12, the CNFs have different orientations in the grains or boundaries, resulting in only parts of the CNFs boring loads effectively.

V. CONCLUSIONS

CNFs/A356 nanocomposites were fabricated by high-intensity ultrasonic processing. Microstructure, mechanical properties, and fracture surfaces were investigated. The results indicated that effective dispersion was achieved by using ultrasonification. The CNFs were well dispersed in the composites prepared using ultrasonic power of 2.1 kW. The mechanical properties of the composites were improved with the increase of ultrasonic power and the CNF content. The UTS (261 MPa) and YS (202 MPa) and microhardness values of the nanocomposite fabricated with 0.9 wt pct CNFs were 21.9, 38.3, and 43.2 pct, respectively, higher than those of the matrix alloy. The thermal expansion mismatch strengthening of the composite, grain refinement of the nanocomposite, and load transfer from the matrix to the nanofibers resulted in significant improvement in the mechanical properties. Therefore, the use of high-intensity ultrasonic processing for the production of high-performance metal composites holds great potential for industrial application.

ACKNOWLEDGMENTS

This research is supported by the National Natural Science Foundation of China (Grant No. 51364035) and the Natural Science Foundation of Jiangxi Province (Grant No. 20171BAB206034).

REFERENCES

1. S. Xie, W. Li, Z. Pan, B. Chang, and L. Sun: *J. Phys. Chem. Solids*, 2000, vol. 61, pp. 1153–58.
2. H. Kwon, G.G. Lee, S.G. Kim, B.W. Lee, W.C. Seo, and L. Marc: *Mater. Sci. Eng. A*, 2015, vol. 632, pp. 72–77.
3. P. Pripanapong, S.F. Li, J. Umeda, and K. Kondoh: *MMSE*, 2016, pp. 2412–5954.
4. F. Ogawa and C. Masuda: *Compos. Part A*, 2015, vol. 71, pp. 84–94.
5. A. Esawia and K. Morsib: *Compos. Part A*, 2007, vol. 38, pp. 646–50.
6. B. Amgalan, I. Batchuulun, U. Batjargal, J.Y. Lee, and H.K. Choi: *Powder Technol.*, 2010, vol. 42, pp. 11–20.
7. X.D. Yang, E.Z. Liu, C.S. Shi, C.N. He, J.J. Li, N.Q. Zhao, and K. Katsuyoshi: *J. Alloy Compd.*, 2013, vol. 563, pp. 216–20.
8. J.J. Moses, I. Dinaharan, and S.J. Sekhar: *Trans. Nonferr. Met. Soc.*, 2016, vol. 26, pp. 1498–1511.
9. X.H. Chen and H. Yan: *J. Mater. Res.*, 2015, vol. 30, pp. 2197–2209.
10. G.I. Eskin: *Ultrason. Sonochem.*, 2001, vol. 8, pp. 319–25.
11. Y. Yang, J. Lan, and X. Li: *Mater. Sci. Eng. A*, 2004, vol. 380, pp. 378–83.
12. C. Sautera, M.A. Emin, H.P. Schuchmann, and S. Tavman: *Ultrason. Sonochem.*, 2008, vol. 15, pp. 517–23.
13. L. Liu, Y.D. Huang, Z.Q. Zhang, and X.B. Yang: *J. Appl. Polym. Sci.*, 2006, vol. 99, pp. 3172–77.
14. Y.L. Li and T.G. Zhou: *Metall. Mater. Trans. A*, 2013, vol. 44A, pp. 3337–43.
15. S.R. Galleguillos, H.Y. Varga, and G.L. Gaete: *Ultrason. Sonochem.*, 2017, vol. 35, pp. 134–41.
16. H. Yan, Z.X. Huan, and H.X. Qiu: *Metall. Mater. Trans. A*, 2017, vol. 48A, pp. 1–9.
17. J.I. Youn, B.I. Kang, D.G. Ko, and Y.J. Kim: *Int. J. Cast. Met. Res.*, 2008, vol. 21, pp. 135–38.
18. Z.W. Shao, Q.C. Le, Z.Q. Zhang, and J.Z. Cui: *Metall. Mater. Int.*, 2012, vol. 18, pp. 209–15.
19. Z.B. Yang, W. Zhou, and P. Wu: *Mater. Sci. Eng. A*, 2014, vol. 590, pp. 295–300.
20. Z.Y. Liu, S.J. Xu, B.L. Xiao, P. Xue, W.G. Wang, and Z.Y. Ma: *Compos. Part A-Appl. S*, 2012, vol. 43, pp. 2161–68.
21. U. Toshiyuki, Y. Takashi, S. Kiminori, M. Yukio, and E. Morinobu: *Jpn. Soc. Powder Metall.*, 2008, vol. 54, pp. 595–600.
22. R. George, K.T. Kashyap, R. Rahul, and S. Yamdagni: *Materials*, 2005, vol. 53, pp. 1159–63.
23. L. Aicha, B.F. Roberto, B. Thierry, B. François, C. Rafik, and G.L. Terence: *Mater. Sci. Eng. A-Struct.*, 2012, vol. 532, pp. 139–45.
24. W. Hu, Z.H. Zhang, H.M. Zhang, Z.Y. Hu, S.L. Li, and X.W. Cheng: 2017, vol. 696, pp. 80–89.
25. H.J. Choi, G.B. Kwon, G.Y. Lee, and D.H. Bae: *Scripta Mater.*, 2008, vol. 59, pp. 360–63.